An Experimental Prediction of the Tropical Atmosphere for the Case of March 1965[1]

K. MIYAKODA, J. C. SADLER,[2] AND G. D. HEMBREE

Geophysical Fluid Dynamics Laboratory, NOAA, Princeton University, Princeton, N. J. 08540

(Manuscript received 31 October 1973, in revised form 18 June 1974)

ABSTRACT

A two-week prediction was made, applying a general circulation model on Kurihara's global grid to an observed data set. The maps for the basic meteorological elements at 10 vertical levels for 5 days in March 1965 were analyzed manually with the aid of nephanalysis charts. This report discusses the forecast results selectively for the tropical areas only. The predicted wind, temperature, and precipitation were compared, whenever possible, with the observed data including satellite cloud pictures. The main objective was to attempt a tropical forecast for a case study, and to obtain a crude idea, based on one sample, about the feasibility of predicting tropical weather systems. Some capability in the prediction of the tropical atmosphere is evident for about 3 days, in particular for the upper troposphere, but the prediction needs considerable improvement for the lower troposphere as well as for the stratosphere.

1. Introduction

The specific questions asked here are: whether tropical disturbances behave systematically or erratically; to what extent the disturbances are predictable; and whether the cloud "clusters" can be predicted deterministically or can only be calculated statistically. To investigate these points or at least to make some approach to these questions, we started to collect meteorological data on a global scale in 1965. The period of the data is March 1965, during which the TIROS IX satellite provided the first daily worldwide cloud mosaics. Meanwhile, in our laboratory, an effort was going on to construct a numerical model of the general circulation with Kurihara's global grid. This model had just reached its first usable stage (Manabe *et al.*, 1970; Holloway and Manabe, 1971; Miyakoda, Moyer, *et al.*, 1971). With these two products a global prediction with real initial data was conducted for a two-week period. This paper discusses only the tropical portion of the experiment.

2. The model

The basic equations and the physics used in the model are nearly the same as those in Smagorinsky *et al.* (1965) and Manabe *et al.* (1965). Some modifications of the physics used are described by Miyakoda, Smagorinsky, *et al.* (1969). The global grid was originally designed by Kurihara (1965) with the idea of having a homogeneous distribution of gridpoints on the sphere. The particular model used here, however, is based on the later version of the Kurihara grid and the finite difference formulation of the equations (Kurihara and Holloway, 1967).

a. Outline

The general characteristics of the model follow: It employs 9 vertical levels (at approximately the 9-, 74-, 189-, 336-, 500-, 664-, 811-, 926-, and 991-mb levels), and makes use of the primitive equations. It is global in extent, with the Kurihara grid, and the horizontal resolution is $N=48$, which means that there are 48 gridpoints between a pole and the equator—i.e., the grid size is 220 km in the meridional direction, but is somewhat inhomogeneous in the zonal direction; and there are 9216 gridpoints per level ($=4\cdot N^2$). It uses the finite difference scheme which guarantees the so-called "kinetic energy conservation" for an appropriate condition. Water vapor is included, as are radiation, orography, and land-sea contrast.

The condensation criterion is 80% relative humidity. The coefficient for nonlinear viscosity is 0.25. The sun's declination is fixed for mid-March. The cloud coverage used for the radiation computation is a function of height and latitude only. The cloud distribution in the Southern Hemisphere was assumed to be equal to the values for autumn in the Northern Hemisphere. Water vapor and ozone as absorbers of radiant

[1] The preliminary report of the paper was presented at the meeting of the American Meteorological Society in New York, 11 January 1969, under the title "Prediction of the Tropical Weather with a Nine-Level Global Model."

[2] Department of Meteorology, University of Hawaii, Honolulu, Hawaii 96822.

energy are also functions of height and latitude, carbon dioxide is a function of height only, and all absorbers are constant with time. Sea surface temperature is supposedly a very important component for the tropical circulation, and in this case it is given by the March normal prepared by the U. S. Navy Hydrographic Office. The ground surface temperature is determined by the heat budget at the surface under the assumption that soil has no heat capacity. The availability of water vapor over sea is 1.0, and that over land is specified as a function of the geographical location, which is based on the climatological values of rainfall. The difference in thermal properties between the land-ice and sea-ice surfaces is taken into consideration. For March, the surface temperatures over sea-ice are set to −29.1C for the Northern Hemisphere and −4.7C for the Southern Hemisphere. The surface drag coefficient over both land and sea is assumed to be 0.002.

It may be useful to note that the following effects were not taken into account: the diurnal and seasonal variations of insolation, the time and space change of albedo due to the deposit of new snow, the response from the ocean, and time and longitudinal variations of cloud cover.

In the following, somewhat detailed descriptions are given of the most important processes in the model related to our tropical problem.

b. Boundary layer process

The turbulent transfer in the surface boundary layer is treated in a simple way. The mixing length is assumed to increase linearly with height from the surface up to the lowest level in the model (level 9, i.e., about 991 mb). Vertical diffusion above level 9 is applied only to momentum so that the mixing length decreases gradually from level 9 to about 700 mb. The eddy coefficient does not include the effect of vertical stratification. No special assumption was made for the Ekman layer representation at the equator.

c. Ensembled small-scale convections

The small-scale convective transfer process, designed by Manabe, is called the "moist convective adjustment" (Manabe *et al.*, 1965). The temperature is instantaneously adjusted to the moist adiabatic lapse rate whenever supersaturation occurs and at the same time the lapse rate tends to exceed the moist adiabatic. The vertical profile of the new temperature is determined in such a way that total energy in the atmospheric column is conserved. The criterion for saturation of humidity was taken in this study to be 80% relative humidity.

It is one of our purposes to investigate the performance of this parameterization scheme by applying it to real data in the tropics. However, a preliminary appraisal of this scheme has already been presented. The most important characteristic of this method is the simplicity of the assumption, the concept, and its practical treatment; and yet this method contains some essential features of the mechanism. Undoubtedly, it provides at least the first approximation of the ensemble effect of cumulus convection. As will be seen later, and also in other articles (e.g., Manabe *et al.*, 1974), there is a body of evidence which tends to show that the performance is not bad.

On the other hand, several shortcomings have also been mentioned:

1) In this method, the subgrid scale convection is assumed to start only if the humidity reaches saturation, whereas in reality the activity seems to occur almost irrespective of the macroscale humidity value.

2) In the lower troposphere of the tropics the temperature profile is often super-moist adiabatic, whereas this method forces the temperature to the moist adiabatic lapse rate in the adjustment process (Krishnamurti and Moxim, 1971).

3) A strong "shock" (geostrophic imbalance) is generated due to a large and sudden change in temperature and moisture (Gadd and Keers, 1970; Miyakoda, Strickler, *et al.*, 1971).

4) In this method all the detailed physical processes are bypassed, and accordingly it is not convenient to make future improvements. For example, the incorporation of momentum transfer in the vertical (advocated by Gray, 1968) is difficult.

d. Remarks on the truncation error

A large truncation error in the Kurihara-grid finite differencing has been pointed out by several authors (see Miyakoda, Moyer, *et al.*, 1971). The present study also has experienced this computational problem. So far as the tropics are concerned, however, the numerical distortion in the solutions is supposedly and hopefully not so enormous. It is noted that after this project was finished the global gridding was modified so that the gridpoints are increased in the zonal direction, but this revised version was not included here.

3. Data, analysis, and initialization

a. Data

Wind, temperature, geopotential height, and moisture data for 10 mandatory levels together with ship and aircraft reports (see Sadler, 1965) were gathered by special request from at least 15 regional data centers with emphasis on the tropics. This arrangement was absolutely necessary to recover the vast amount of missing data in routine communication. The period for the data set is 5 days commencing at 00 GMT 1 March 1965. The cloud pictures televised

from the TIROS IX satellite were utilized in the analyses. Usability of the radiometer data from the TIROS VII satellite for the determination of the stratospheric temperature was examined, but it appeared that the data deterioration for that period was too large. The moisture analysis was mainly determined from the satellite observed cloudiness.

b. Analysis

The data were plotted on Mercator projection maps at 24-hr intervals. The off-time data were used over data-sparse regions and for time continuity. Analysis was performed subjectively for the streamlines, isotachs, temperature, humidity, surface pressure, and height of constant pressure surfaces for the belt between 40N and 40S. These were meshed with the Northern and Southern Hemisphere analyses to obtain a consistent tropical boundary at 30N and 30S.

Fig. 1 is the streamline analyses for the 200-mb, 700-mb, and surface levels at the initial time, i.e., 00 GMT 1 March. In the maps, the anticyclones are denoted by an *A*, and the cyclones by a *C*. When a vortex is located just at the equator, it is labeled *E*. In the Southern Hemisphere the summer monsoon is very strong over the Indian Ocean and western Pacific. The circulation is more typical of mid-February than March. The low-level westerlies extend from Africa eastward to 180° with an observed speed at 850 mb (not shown) of 35 kt at both Diego Garcia (7S, 72E) and Djakarta. These westerlies are also abnormally deep as indicated by the 500-mb observations of 35 kt and 30 kt at Diego Garcia and Darwin, Australia, respectively. Two tropical cyclones of hurricane intensity had developed earlier in the *monsoon trough* over the south Indian Ocean and on the 1st of March are recurving poleward. Hurricane Dolly is located just west of Australia and hurricane Gay near 75E. Hurricane Gay crossed the 70E meridian and was renamed Olive on the 2nd of March. The eastern end of the monsoon trough has the typical orientation from New Guinea southeastward across 180° near 30S. Numerous cyclonic vortices, other than the two hurricanes, existed in the monsoon trough; however, none was of sufficient intensity to maintain a definite time and space continuity for the 5-day period.

The Southern Hemisphere *tropical upper tropospheric trough* (*TUTT*) at 200 mb is near its normal position (Sadler, 1972) extending southeastward from the equator at 170W. The trough is rather intense as indicated by the associated low-level cyclonic systems. During the 5 days a family of surface vortices was initiated in the longitude of 150W-120W. The satellite data would support at least a tropical storm intensity for one of the systems on the 3rd of March and the nearest surface observation had a speed of 35 kt.

In the Northern Hemisphere the low-level "buffer system" (a counter-clockwise turning wind system between the monsoon westerlies of the Southern Hemisphere and the tropical easterlies of the Northern Hemisphere; see Sadler and Harris, 1970) lies north of the equator as a trough in the western Pacific. A tropical depression in the eastern end of the trough near 4N and 145E, on the 1st, drifted westnorthwest to 8N and 130E by the 5th. The major mid-latitude interactions with the tropics were a moderate northeast monsoon surge into the South China Sea and western Pacific on 4 and 5 March and a deep upper trough in the westerlies with a cut-off low just east of the Hawaiian Islands.

It is noted that Krishnamurti (1969), in his prediction experiment, used the initial condition for the same day, i.e. 1 March 1965, but for 12 GMT (our case is for 00 GMT). Although the domain of his maps is smaller, his analysis can be compared with ours. There are quite a few differences.

The maps were then digitized with a graphic data digitizer, which gives the values of any scalar or vector, at 181×31 gridpoints, 2° interval (valid on the equator), on the 30N–30S Mercator map. The 2° grid spacing was adopted without profound consideration, but as will be mentioned later, this resolution happens to be adequate for the representation of streamlines at the 700-mb level; 4° resolution is not satisfactory. There is another aspect. Hayden (1970) found that the predominant width of "cloud clusters" is 275 km in winter and 450 km in summer, and based on this, suggested that the grid size in the tropics should be equal to or less than 2°. The grid we are discussing, of course, is not the "computational grid" used in a prediction model, but the "data grid" used for the map representation of the weather system, though in our particular case both grid resolutions happen to be the same.

Persistence, i.e., day-to-day continuity, and internal consistency checks of the analyzed maps were performed—i.e., the streamlines against the cloud pictures, consistency checks of the wind fields and geopotential height fields by solving the balance equation from wind to geopotential (Miyakoda, 1960), and hydrostatic consistency between temperature and thickness (see Bedient and Vederman, 1964, for an example of objective tropical analysis).

The data outside the tropical area were taken from three sources. The Northern Hemispheric troposphere was taken from the objective analysis of the National Meteorological Center, Suitland, Md. The stratospheric maps for the Northern Hemisphere, of geopotential height and temperature, were taken from the published analysis of Berlin Freien Universität. The Southern hemispheric troposphere and stratosphere were analyzed subjectively by Clarke (Clarke and Strickler, 1972). These maps of different sources were assembled with a degree of compromise at the boundaries.

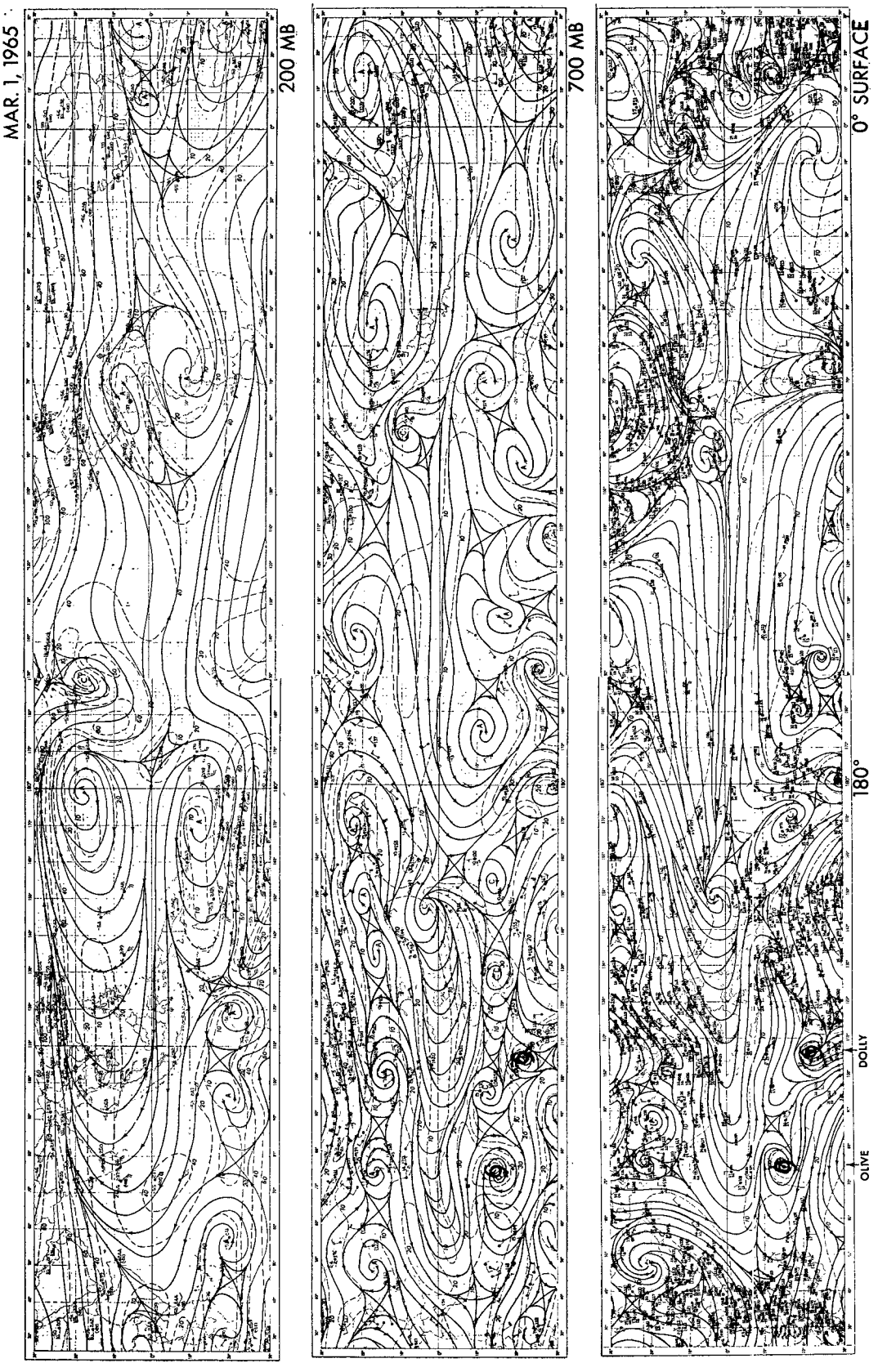

FIG. 1. Examples of streamline and isotachs patterns for 200 mb, 700 mb, and surface levels at the initial time. The units of the isotachs are knots.

c. Initialization

The conventional method of initialization was employed to adjust the data for the prediction computation, not because this old method is satisfactory, but because a more advanced method was not available at that time (for example, the "4-dimensional" analysis).

For the areas poleward from 15N and 15S, the conventional process was applied for the Northern and Southern Hemispheres, respectively; that is, the *balance equation* and the *ω-equation* were used to derive the rotational and the divergent components of wind from the geopotential height. On the other hand, in the tropical region, the analyzed wind was used directly. So the divergent component was automatically included in the tropics at least in principle, regardless of its reliability. The temperature field was compared and made essentially consistent with the geopotential and, accordingly, the wind field was checked for geostrophic balance and hydrostatic balance. The data thus processed for the middle and high latitudes and for the tropical belts were smoothly connected at around the 30N and 30S latitude circles.

Using these initial conditions, a marching calculation of the prediction was carried out with Matsuno's Euler-backward time differencing technique (Matsuno, 1966) for the first half day. The tropics present unique and formidable problems in initialization: one factor is the large amount of condensation heat as well as the associated tropical disturbances; the second factor is the weak control on motions due to the lack of the earth's rotational effect in the equatorial region; and the third factor is the presence of medium scale intense motion systems such as hurricanes. These factors make the initialization extremely difficult, and the conventional technique cannot accomplish the complete balancing. The application of the Matsuno scheme is a quick remedy for suppressing the unreasonably large oscillations. After one-half day, the Euler-backward process was changed to the usual leap-frog method (centered difference). The prediction computations were made in 1968 with the UNIVAC 1108, which used 31 hours' computer time for a one-day forecast. The predictions were made for 14 days.

4. The zonal and temporal means

Let us first look at the solutions of the prediction averaged zonally and temporally for the period from the 4th through the 14th day. The reason for excluding the first 3 days is to avoid the transient state of the solutions during the initial adjustment period. Figs. 2, 3, and 4 provide the meridional sections for the temperature, zonal wind, and relative humidity.

The predicted winds (Fig. 3) deviate in significant aspects from the observed of the initial day. Some deviation is expected but the persistent primary currents should be retained. The most obvious error is the elimination of the lower stratospheric core of westerlies centered at 20 km, i.e., the "Berson westerlies." More significant to synoptic systems is the over forecast of the low-level easterlies. The monsoon westerlies, a persistent and most important feature of this season, have been weakened or eliminated since by the third-day forecast they were replaced, contrary to observations, by easterlies in the longitudes of 135E to 180°. Even the Northern Hemisphere easterlies which were observed as being stronger than normal on the initial day (7.1 m sec^{-1}) were further intensified by the forecast to an unreasonable zonal average of 8.4 m sec^{-1} in comparison with seasonal means of

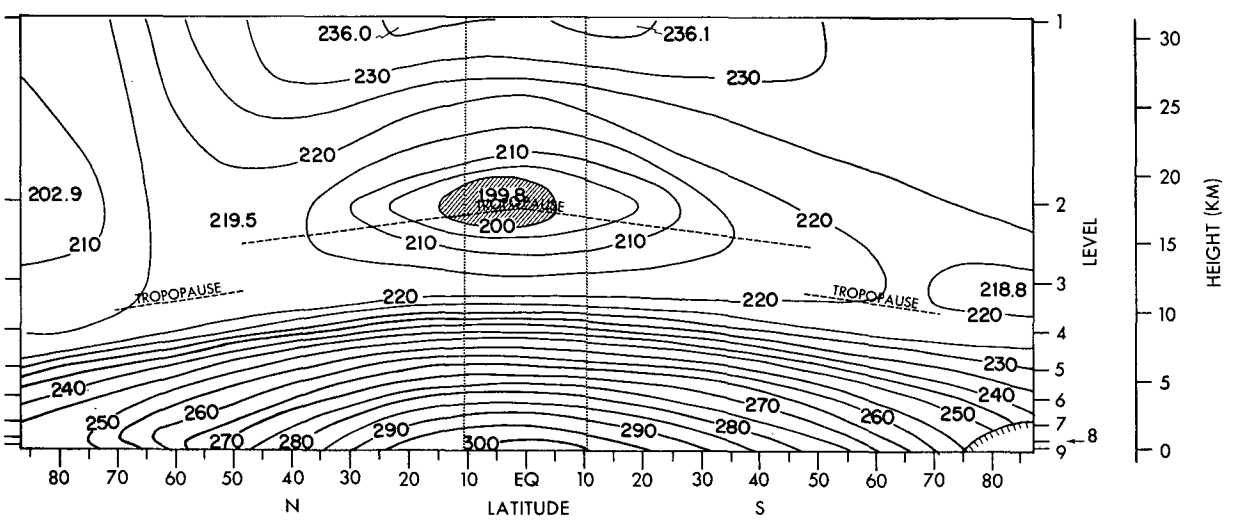

FIG. 2. Predicted temperature zonally and temporally averaged for 10 days in units of °K. The extrema are plotted. The vertical dashed lines at 10N and 10S indicate the equatorial region, where the comparison between the forecast and observation is made.

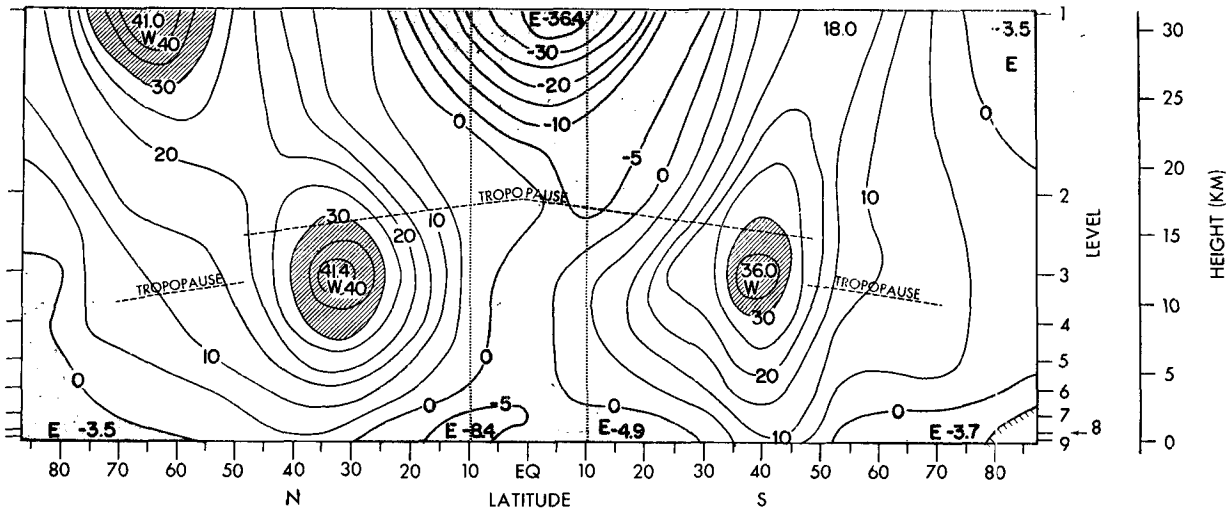

FIG. 3. Predicted west-east component of wind zonally and temporally averaged for 10 days in units of m sec^{-1}. The W's are the westerlies and E's are the easterlies (negative).

near 3 m sec^{-1} (Kidson *et al.*, 1969) and the March mean of near 4 m sec^{-1} at the gradient level (Atkinson and Sadler, 1970).

The predicted humidity (Fig. 4) shows a large deviation from reality. The near surface values are symmetrical about the equator between the 40th parallels. Along the 20th parallels, the winter desert conditions typical of Africa, Arabia, India, Indochina, and Mexico comprise more than one-third of the global circumference at 20N and should have values different from those at 20S where the smaller land area is within the humid tropics. The maximum humidity centered on the equator appears contrary to observations of rainfall and cloudiness, as will be discussed later, and the value in the upper troposphere is excessive when compared to mean conditions (Kidson *et al.*, 1969).

Exact comparison with observation, however, is not possible, because the analyzed maps are only for the first 5 days, although station data are available for the entire 14-day period. In order to make a comparison as objective as possible, the following approach was used. First, the available observational data are taken for the zonal belt between 10N and 10S on the pressure levels 1000, 850, 700, 500, 300, 200, 100, 50, 30, and 10 mb. In a similar way, the predicted values at the nearest grid points to these observation stations are interpolated for the same pressure levels. For both the forecast and the observation, the values for temperature, zonal wind, and humidity were averaged arithmetically for the 10-day period, i.e., days 4–14. Figs. 5, 6, and 7 show the results as a function of pressure. It turned out that each day there are about 20 stations in this belt that reported

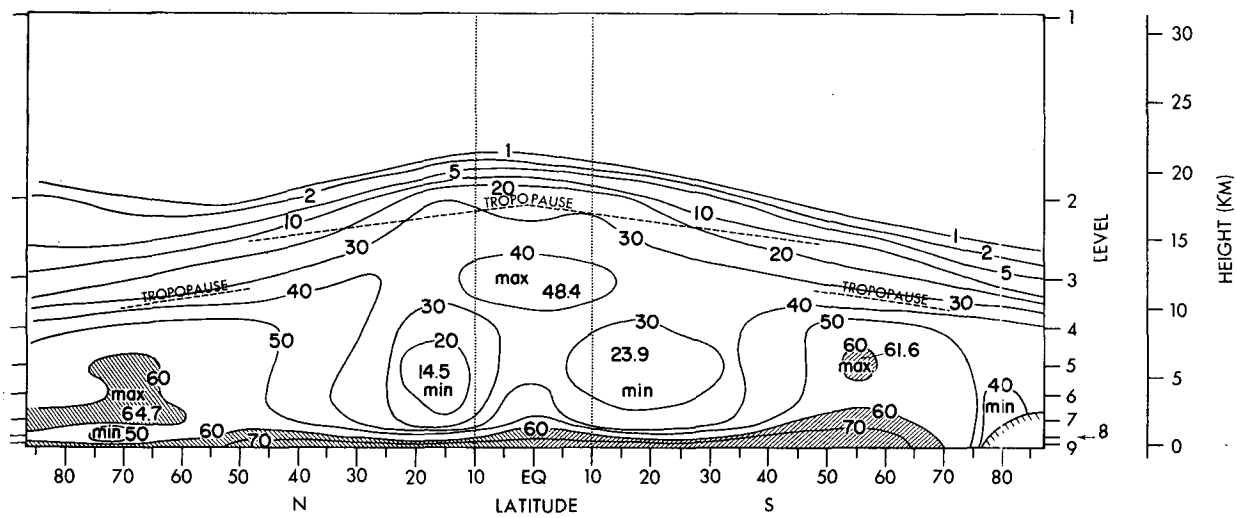

FIG. 4. Predicted relative humidity zonally and temporally averaged for 10 days, in percent.

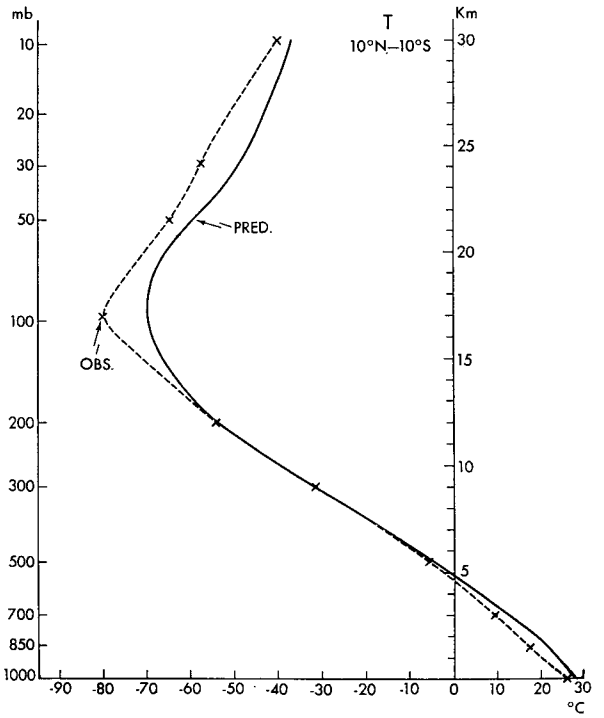

FIG. 5. Comparison of the vertical distribution of temperature between forecast (solid lines) and observed (dashed lines) values for the equatorial region, averaged for 10 days, in °C.

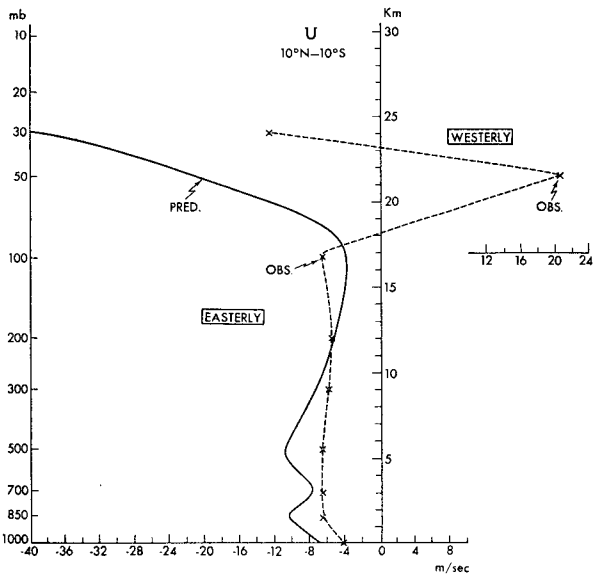

FIG. 6. Comparison of the vertical distribution of the west-east component of wind between forecast (solid lines) and observed (dashed lines) values for the equatorial region, averaged for 10 days, in units of m sec^{-1}.

data for the levels below 200 mb, and there are less in the stratosphere, i.e., 10 stations at 50 mb and only 2 at the 10-mb level. As a check, one may compare the predicted values in these figures with those in the meridional sections, Figs. 2, 3, and 4, where the 10N–10S regions are marked by dashed lines. The values do not always coincide, indicating that the data selected for Figs. 5, 6, and 7 are not a sufficiently large sample, but more specifically, the fixed observations are not well distributed throughout the longitudes. Despite this discrepancy it is hoped that the comparison between the prediction and the observation is meaningful.

Fig. 5 is the comparison for the temperature: the predicted temperature is higher than the observed. This is particularly so near the tropopause level; there the difference is about 10C. It is interesting to note that in the middle and high latitudes the disagreement is just the opposite (not shown here); there, the predicted atmosphere appears generally cooler than the observed. The reason for the lower temperature in the higher latitudes is apparently due to the inaccuracy of the radiation calculation, whereas the reason for the discrepancy in the lower latitudes is not yet clear. It is also noticed in Fig. 5 that the predicted temperature in the low levels is erroneous, being higher than the observed.

Fig. 6 is the comparison for the zonal wind. Overall, the zonal wind was simulated to some extent, but some differences were recognized. The most obvious difference between prediction and observation is in the stratosphere. The stratospheric wind systems of the equatorial region are highly zonal (see Sadler, 1957) and vary only slowly with time through a quasi-biennial cycle; therefore, the few observations are a good representation of the zonal time mean for the 10-day period. The predicted stratospheric easterlies

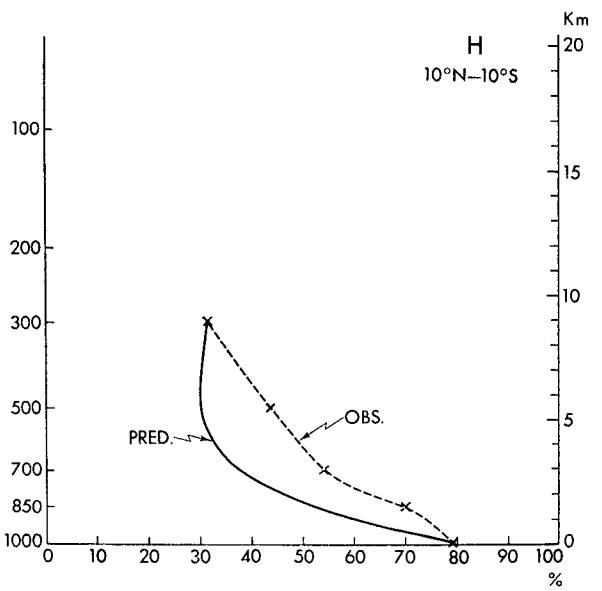

FIG. 7. Comparison of the vertical distribution of relative humidity between forecast (solid lines) and observed (dashed lines) values for the equatorial region averaged for 10 days, in percent.

are much too strong and even eliminated the observed westerly core centered near 20 km. Conceivably this error is not negligible, because the vertical shear in wind may cause a considerable effect on the wave dynamics in the equatorial region. These results altogether indicate that the vertical resolution of the model at the tropopause level as well as in the stratosphere is insufficient.

The observations of Fig. 6 within the troposphere are considerably biased by the distribution of observation points. In the upper troposphere the observed relatively strong westerlies covering most of the western hemisphere which dominated the zonal average above 14 km are observed only by aircraft and therefore are not sampled in Fig. 6. The monsoon westerlies of the lower troposphere over the South Indian Ocean and the western South Pacific are sampled by no more than three of the twenty stations. More observations in these two major currents would reveal a greater deviation between the observed and predicted curves throughout the troposphere.

The observed moisture decreases very rapidly with height in the lower levels (Fig. 7), due probably to the concentration of stations in the Northern Hemisphere sampling the typical trade wind moisture profile over the oceans (Malkus, 1962) and dry continental air over land. Even with this bias, the prediction is much lower than the observed. This result is also opposite to that in the middle and high latitudes. However, as was discussed elsewhere (Miyakoda, Strickler, *et al.*, 1971), the humidity is affected appreciably by the horizontal grid resolution, and hence any final conclusion should be reserved until an experiment with a more refined grid model is carried out.

Next, we shall take a look at some other variable which is important to the study of tropical dynamics, but which has no observational counterpart for comparisons. Fig. 8 is the meridional section for the predicted vertical velocity, which is averaged in the same way as the previous quantities.

The Hadley circulation is the most dominant and therefore most important component of motion in the tropics. The maximum upward motion in the zonal mean is located right at the equator in this case and the intensity is 1.1 cm sec^{-1}. This location conflicts somewhat with the observed cloudiness, which will be discussed in a later section. The magnitude of 1.1 cm sec^{-1} is about 3 times the March mean of Oort and Rasmusson (1970). One of the peculiar features in the vertical velocity is that there is a sinking current at the tropopause level in the equatorial region. The intensity of the downward current is 0.06 cm sec^{-1} in the zonal and time mean (see Fig. 8). It is interesting to note that this downward current existed also in previous results (see Wetherald and Manabe, 1972, and Miyakoda, Moyer, *et al.*, 1971). Also in the "dry" global circulation experiment by Kurihara and Holloway (1967), the downward flow is present, though it is feeble. We will discuss this phenomenon further in Section 7.

5. Flow fields

Within the tropics, the zonal average is less than satisfactory for depicting the overall tropical tropospheric circulation, since there is a wind reversal with longitude. For example, winds are in opposite directions over the monsoonal eastern hemisphere and the trade wind western hemisphere, so that the true strength of the currents is masked by zonal averaging. Therefore, let us look at the horizontal distribution of the flow.

a. Representation of maps

In middle and high latitudes it is customary to use the geopotential height maps for the presentation of forecast results, but in the tropics this field is not appropriate because its spatial variation is small. Instead, the streamline pattern is used more frequently.

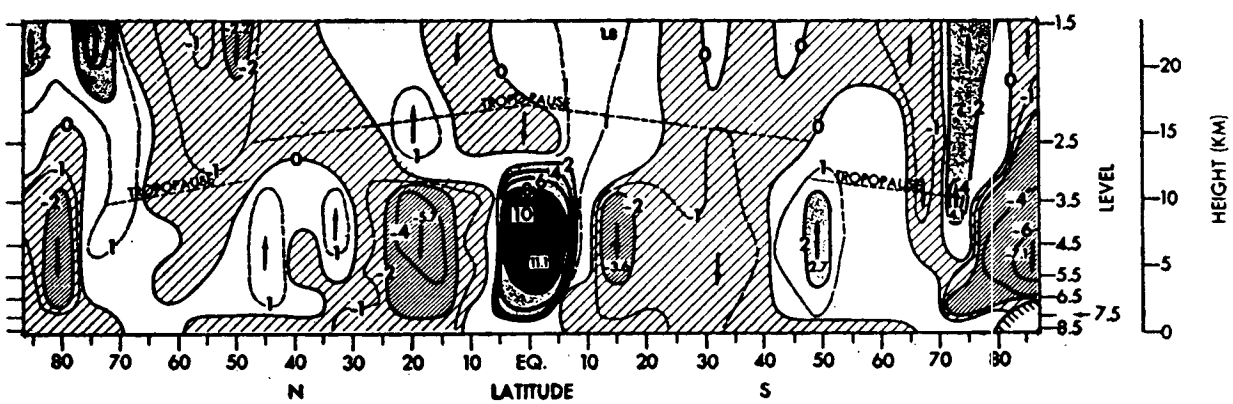

FIG. 8. Predicted vertical velocity zonally and temporally averaged for 10 days in units of 10^{-1} cm sec^{-1}. The arrows indicate the upward and downward motions.

The streamlines in the figures shown below are generated by selecting points randomly from the total domain and by tracing these points in a Lagrangian way with the existing flow field, which is assumed stationary only for the purpose of constructing the streamlines. Fig. 9 shows streamlines at the 200-mb level. The maps at the initial time correspond to the maps that were subjectively analyzed and drawn manually (Fig. 1). As mentioned earlier, the streamlines that are drawn by machine are based on the digitized wind velocity for the 2° interval grid. The representation of the streamlines appears satisfactory, but if the data are given for the 4° interval grid the resemblance is not good; many vortices are filtered out.

The only problem is that for quantitative verification, streamlines are not appropriate; for this purpose the streamfunctions and the velocity potential fields are suitable. The zonal and meridional components of wind vector u, v are written in terms of the streamfunction ψ and the velocity potential χ as

$$u=-\frac{\partial\psi}{a\partial\varphi}+\frac{\partial\chi}{a\cos\varphi\partial\lambda}, \tag{1}$$

$$v=\frac{\partial\psi}{a\cos\varphi\partial\lambda}+\frac{\partial\chi}{a\partial\varphi}, \tag{2}$$

where a is the radius of the earth and λ and φ are the longitude and latitude respectively. From (1) and (2), the vorticity equation is derived as

$$\nabla^2\psi=F, \tag{3}$$

where

$$F=\frac{1}{a\cos\varphi}\frac{\partial v}{\partial\lambda}-\frac{\partial(u\cos\varphi)}{a\cos\varphi\partial\varphi} \tag{4}$$

and

$$\nabla^2=\frac{\partial^2}{a^2\cos^2\varphi\partial\lambda^2}+\frac{1}{a^2\cos\varphi}\frac{\partial}{\partial\varphi}\left(\cos\varphi\frac{\partial}{\partial\varphi}\right). \tag{5}$$

The streamfunction (ψ) is obtained by solving the Poisson equation (3) under the assumption that F is given for the zonal belt encircling the globe between the latitude $+\varphi_1$ and $-\varphi_1$; in practice, φ_1 is taken as 35°. The boundary conditions for ψ are

$$\psi_N=\bar{\psi}_N+\frac{gz}{2\Omega\sin\varphi_1} \quad \text{at} \quad \varphi=+\varphi_1, \tag{6}$$

$$\psi_S=\bar{\psi}_S-\frac{gz}{2\Omega\sin\varphi_1} \quad \text{at} \quad \varphi=-\varphi_1, \tag{7}$$

where $\bar{\psi}_N$ and $\bar{\psi}_S$ are the zonal means to be obtained below, z is the geopotential height, g is the acceleration of gravity, Ω is the earth's rotation, and $\bar{\psi}_N$ and $\bar{\psi}_S$ are derived from (1), i.e.,

$$\bar{\psi}_N-\bar{\psi}_S=\frac{a}{2\pi}\int_{-\varphi_1}^{+\varphi_1}\int_0^{2\pi}ud\lambda d\varphi. \tag{8}$$

In practice, we set $\bar{\psi}_S=-\bar{\psi}_N$.

Maps of the streamfunctions are illustrated in Fig. 10, but maps of the velocity potential are not shown here. This kind of streamfunction presentation was also used by Krishnamurti (1969) and Vanderman (1972); the velocity potential maps were effectively used by Krishnamurti (1971). Our streamfunction map for the 0th day in Fig. 10 was compared with the similar chart for 12 GMT of Krishnamurti (1969); the agreement is not good.

b. 50-mb fields

The forecast of 50-mb flow patterns is a complete failure; the forecast patterns are quite different from the "observed" (or analysis) even at the 1st day. This is probably because of the insufficient vertical resolution of the model.

c. 200-mb fields

Figs. 9 and 10 are the 4-day evolutions of 200-mb flow fields both for the observation and the forecast. The overall resemblance between them is not bad, though it is by no means excellent. The forecast skill is not high by the usual yardstick for middle latitudes, so we did not attempt any quantitative verification of the prediction.

The subtropical ridges are reasonably forecast in the eastern hemisphere with only minor disagreements in latitudinal position. The TUTT, extending southeastward from near 170W at the equator to 135W at 30S is maintained quite well in the forecast field. The most significant disagreement is the movement westward of the South American anticyclonic cells. These are supposedly maintained by the large convective heat source and should remain essentially stationary over the continent. A spurious anticyclonic cell appeared on the 3rd day forecast near 5S and 65E.

d. 700-mb fields

The results for the 700-mb level are shown in Fig. 11. Compared with the 200-mb flow fields, these maps include perturbations of considerably smaller scale. Some irregularities are fictitious, and they are due to the sudden adjustment for convection.

There are some large-scale agreements between the observed and forecast field, particularly after the first day. On the first day there appears to be erroneous cross-equatorial flow in the Pacific (not seen in Fig. 11); it was caused by the incomplete initialization of data. There is considerable similarity in the mainte-

nance of the subtropical ridge over the eastern hemisphere north of the equator and over southern Africa. The primary westerly monsoon current is forecast with reasonable accuracy over the South Indian Ocean between the equator and 15S; however, the cyclonic cells within the monsoon trough, including hurricanes Dolly and Olive, are not well maintained in the surface field (not shown here). Their movement is forecast in general agreement with observations. Hurricane Olive moved southward from 10S and reached 25S on the 4th day. Hurricane Dolly was originally located at 20S, and moved to 27S by the 3rd day, and it disappeared on the 4th day. In the surface level prediction, it moved to about 25S on the 3rd day, and it disappeared on the 4th day. However, at 700 mb the tropical storms tend to be dispersed quickly, mainly because of truncation error and also probably due to the inadequate initial conditions for the thermal and dynamical structure of hurricanes. Miller (1969) reported that with a grid resolution of 140 km in the horizontal and 7 vertical levels, a certain degree of success was achieved in forecasting the movement and even the development of hurricanes 24 hours ahead. Manabe *et al.* (1970), on the other hand, performed a global circulation experiment with a 4° mesh, and found that a number of hurricane-like disturbances

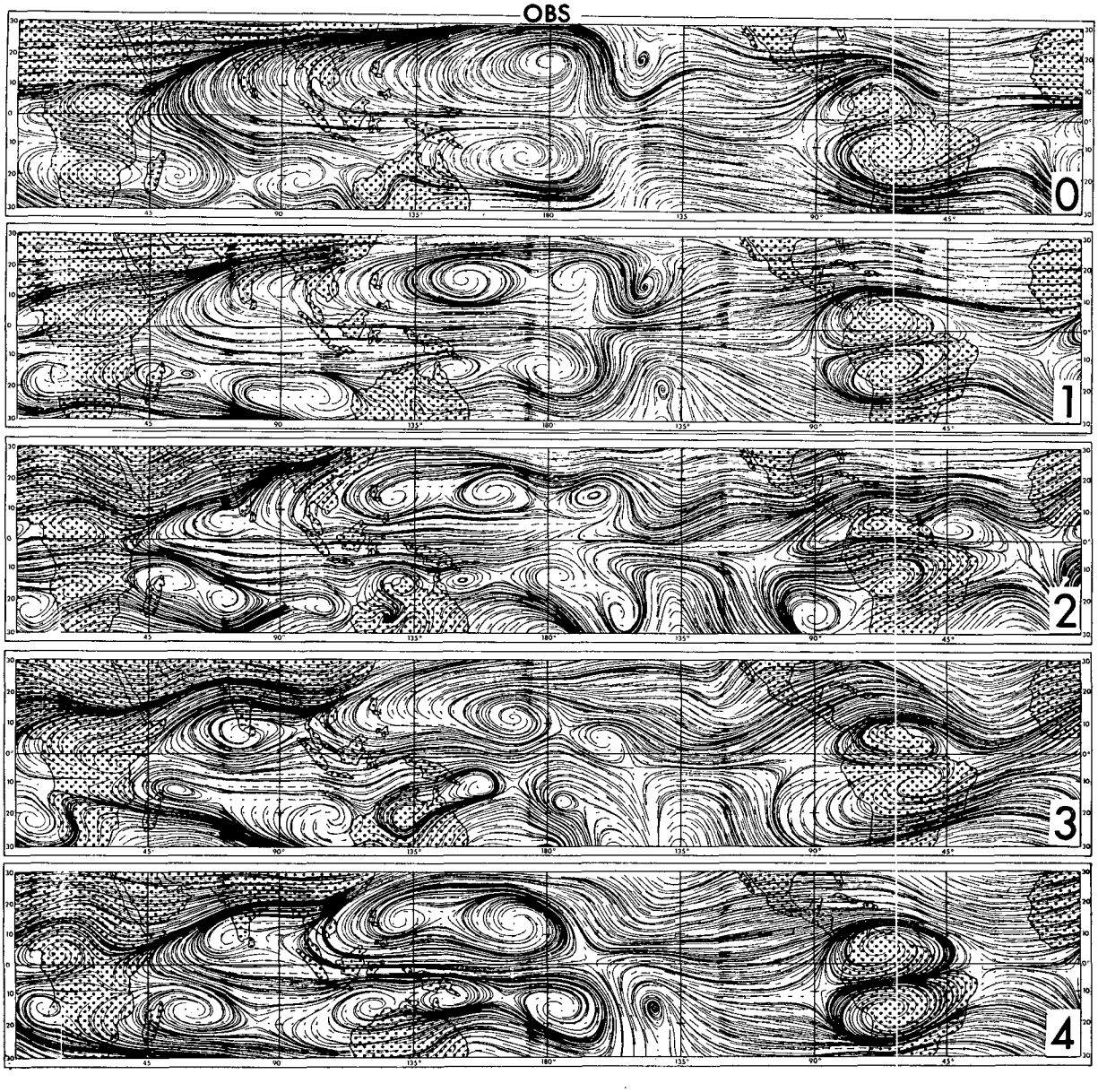

were formed in the areas which coincide with the climatologically favorable region of hurricane formation (Gray, 1968). This may imply that even with a coarse mesh, such as 4°, hurricanes are generated in the course of computation presumably if necessary meteorological conditions are met, and that the computed tropical cyclones are preserved, if the necessary structure is contained in the model, though they may be unrealistically shallow.

In order to make a precise forecast of tropical storms and to extend the forecast period longer than Miller's case, a finer grid may be needed. Ooyama (1969), in the model designed to treat a single isolated hurricane system, used a mesh of 20 km or even 5 km in the central regions of the storm.

The extension of the monsoon trough from northeast of Australia southeastward to near 180° and 30S is gradually eliminated in the forecast. In fact, by the 3rd day the observed trough is replaced by a ridge in the forecast and a well defined cyclonic cell is replaced by an anticyclonic cell near 14S, 160E.

6. Precipitation

A verification of predicted rain against observed cloudiness is the best global comparison that is observationally available at present. However, since they are different variables, the interpretation needs special care and an exact coincidence between these two patterns should not be expected.

a. Zonal mean

The 10-day means of the predicted rain and of the observed clouds are averaged zonally, and compared with other quantities in Fig. 12. The curves include the model's rainfall; the satellite cloudiness for the same period (the curve marked Sadler); the brightness from another satellite, obtained by Winston (1971) for March; and the convergence of the observed water vapor obtained by Rasmusson (1973) based on five-year data for March. Note that the latter two quantities are not for the same period as the one we are treating.

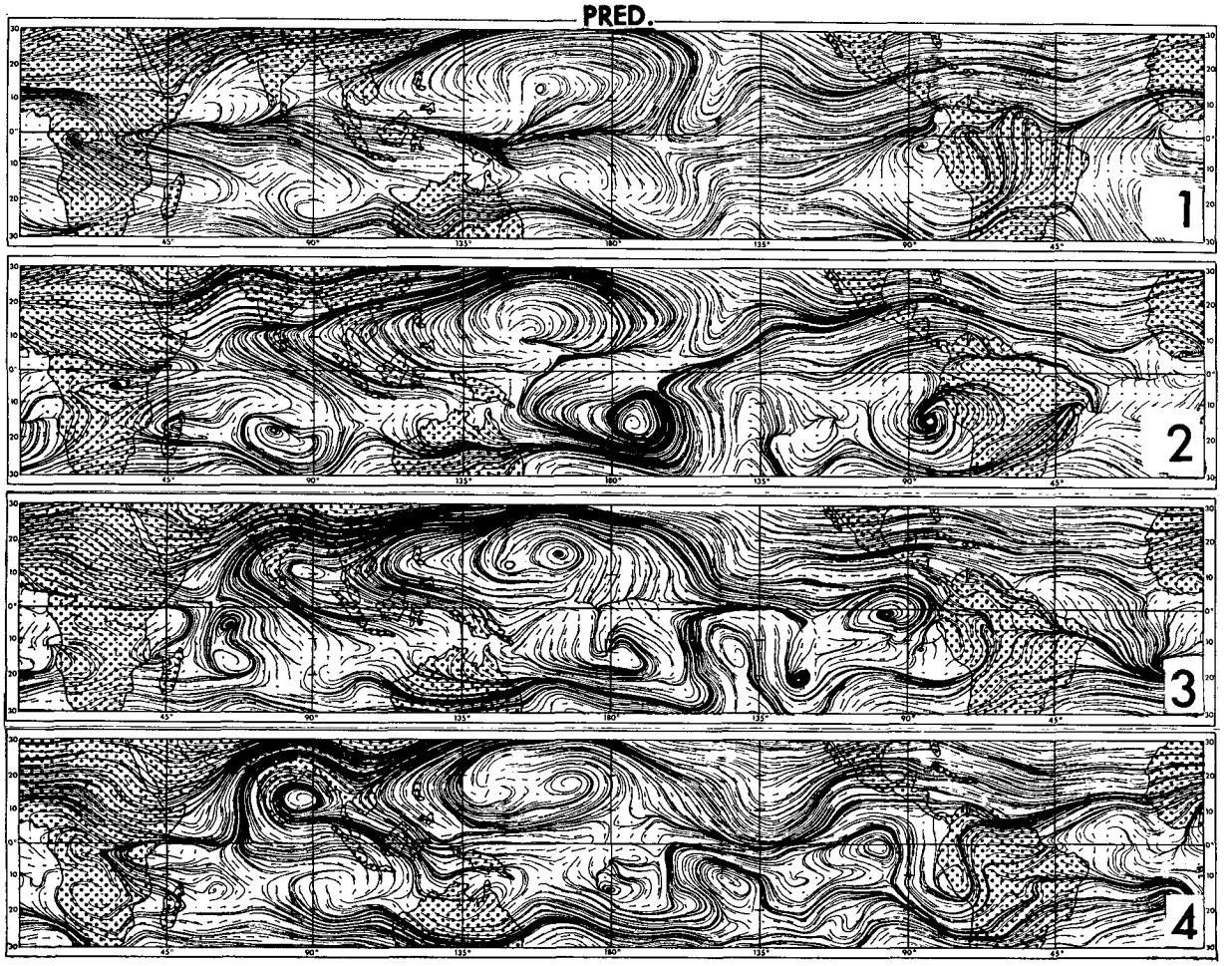

FIG. 9. Comparison of the streamline patterns for 4 days at the 200-mb level: forecast patterns (right) and observed (left).

Two pronounced facts may be noted in the figure: a) in the latitudinal distribution of all the quantities except the predicted rain, there are relative minima right at the equator; b) in the Southern Hemisphere, the rain forecast appears too small compared with the cloudiness and the water vapor convergence. Concerning the first point, the coincidence of the relative minimum with the equator is due to zonal averaging. In the central and eastern Pacific and the Atlantic the minimum is slightly south of the equator and in the west Indian Ocean and Africa it is north of the equator. The causes of the minimum are a matter of debate, many hypotheses having been postulated for the formation and maintenance of the ITCZ (or a maximum cloud zone) and the perhaps associated relative minimum zone (Charney, 1966; Bates, 1970; Holton *et al.*, 1971; Yamasaki, 1971; Hayashi, 1971; and Pike, 1972). The reason for the deficiency of the present prediction will be discussed in *Remarks* below. With respect to the second point, it is now accepted that the March cloudiness is substantially greater in the Southern Hemisphere than in the Northern Hemi-

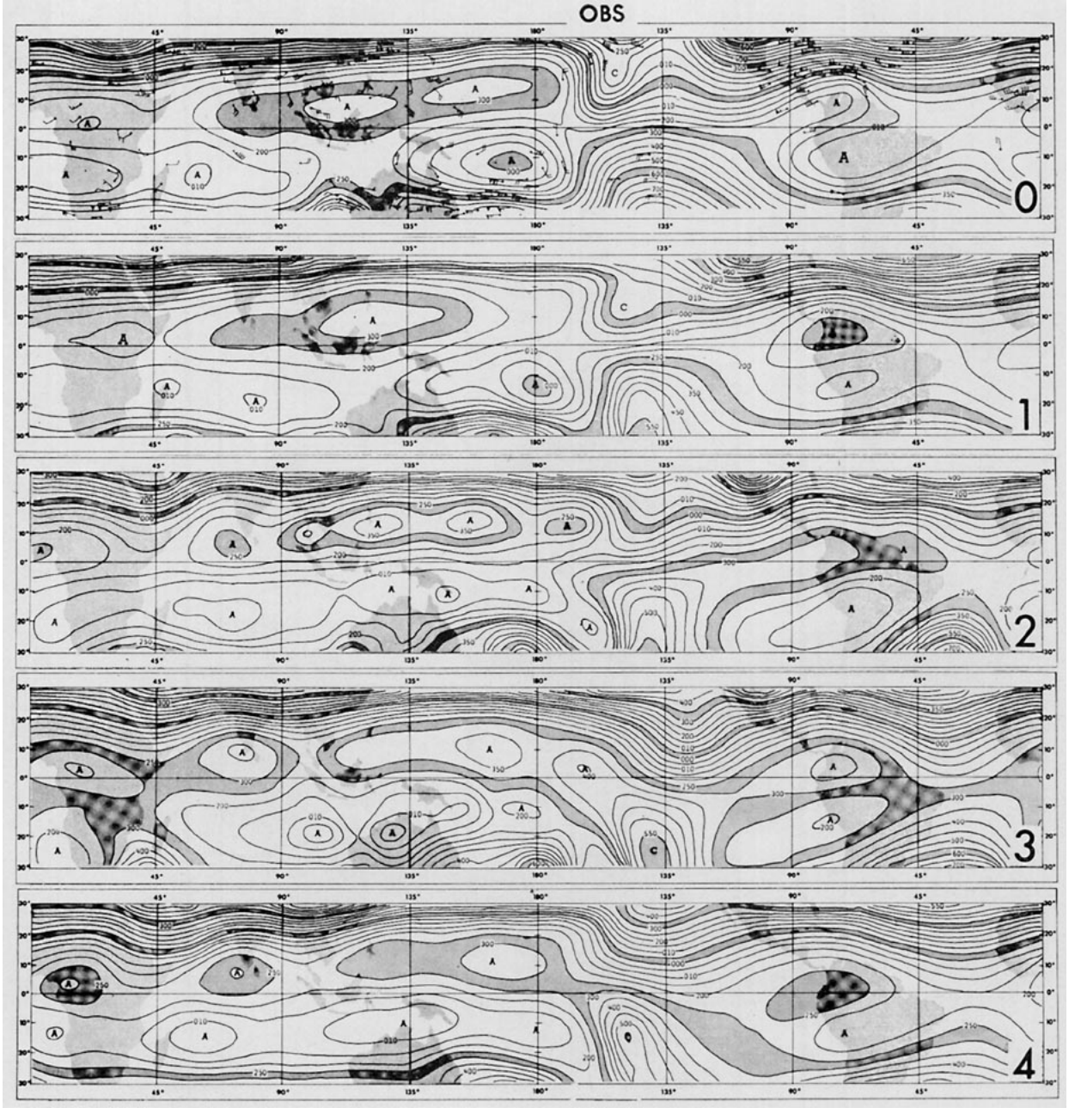

sphere (Sadler, 1969) and also that the rainfall has a similar tendency (see Riehl, 1954, page 77).

b. The daily patterns

Fig. 13 is the series of patterns of predicted condensation as well as the cloud coverage obtained by the TIROS IX satellite. The maps are the 30N–30S Mercator projection maps and the geography is shown in the pattern at the bottom. The six maps show the time evolution of the rain distribution, commencing on the 0th day, i.e., 1 March 1965, until the 5th day. The precipitation is indicated by the contoured lines and the area in which the rain is more than 1/4 inch is shaded lightly. For example, the pattern for the 0th day contains the integrations of rain from 00 GMT 1 March through 00 GMT 2 March. The cloud distribution is based upon the cloud coverage which was observed by the orbiting satellite and was scanned only once a day. The region in which the cloud category of the nephanalysis is C and C+ is shaded black.

So far as the 0th day is concerned, the agreement between the two patterns is good. For instance, on the 0th day, the so-called "convex band" of clouds in the South Pacific near the Solomon Islands is in good agreement. This precipitation is very similar to that of Krishnamurti (1969) in the same domain as in his case. The precipitation patterns in our case deviate with time. One characteristic is that at the beginning of the forecast the computed precipitation is well organized, but as time goes on, say after the 3rd day, the predicted rain is very "spotty." The spotty pattern is probably due to the shortcomings of the parameterization for cumulus convection. In particular it may be related to the "shocking" caused by the sudden adjustment. In any event, the good agreement between rain and cloudiness on the first day is most encouraging. It may imply that the

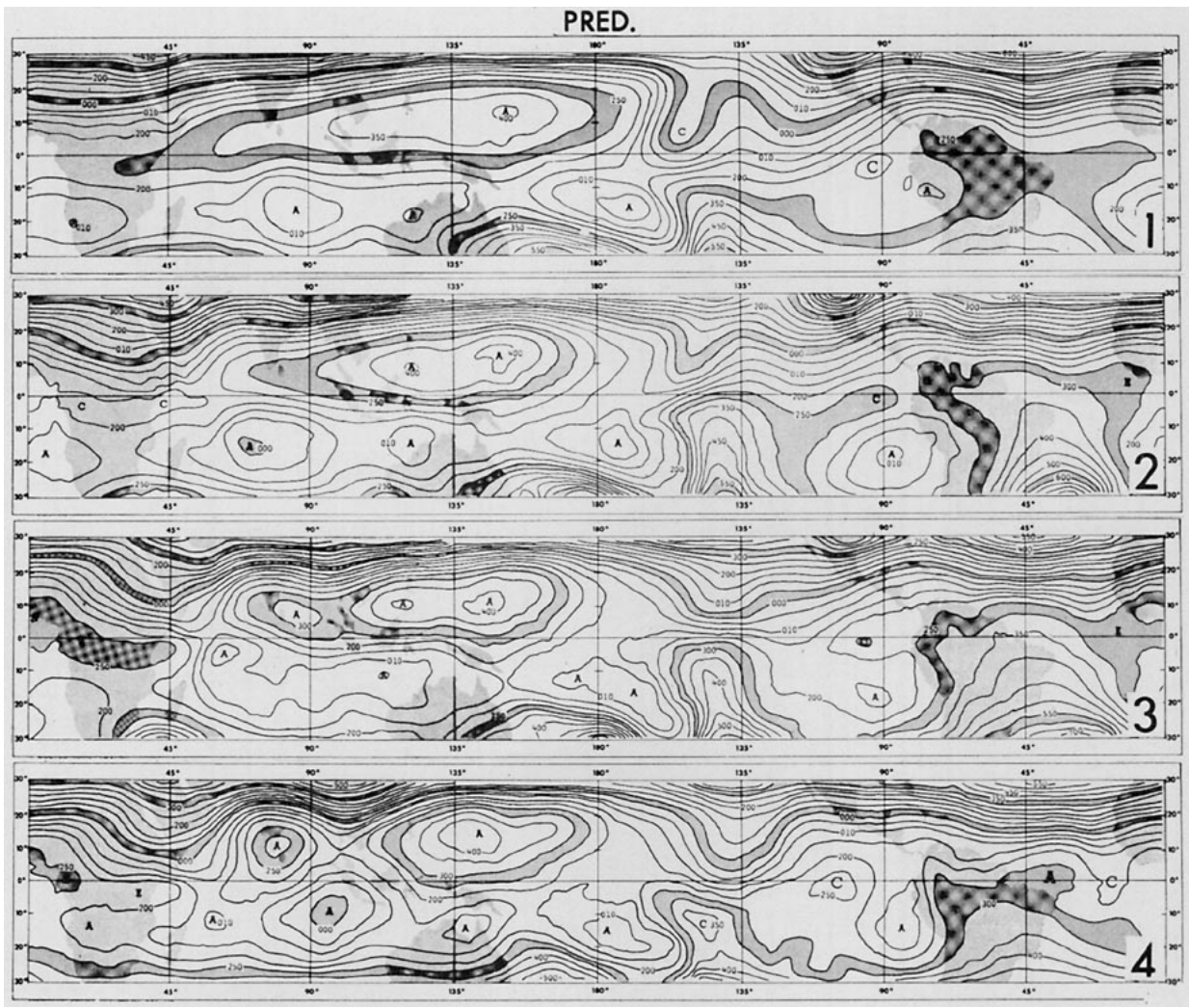

FIG. 10. Same as in Fig. 9, but for the streamfunction. The station data are plotted on the 0th day map.

"subjective" tropical analysis at initial time is not bad, and that the "moist convective adjustment" is capable of yielding a correct forecast of condensation to this accuracy at least.

c. Remarks

The above results indicate that the present model has a tendency to produce rain concentrated at the equator, which is a deviation from reality. This deviation appears to be due to the general inability of the model to predict the circulation patterns since the precipitation forecast for the first day based on analyses is surprisingly good. A number of possible causes for the deterioration can be considered; e.g., an error in the sea surface temperature, a defective boundary layer assumption, an improper parameterization of cumulus convection, an inadequate vertical and spatial resolution particularly for moisture, etc. It was suggested by Manabe *et al.* (1974) that the concentration

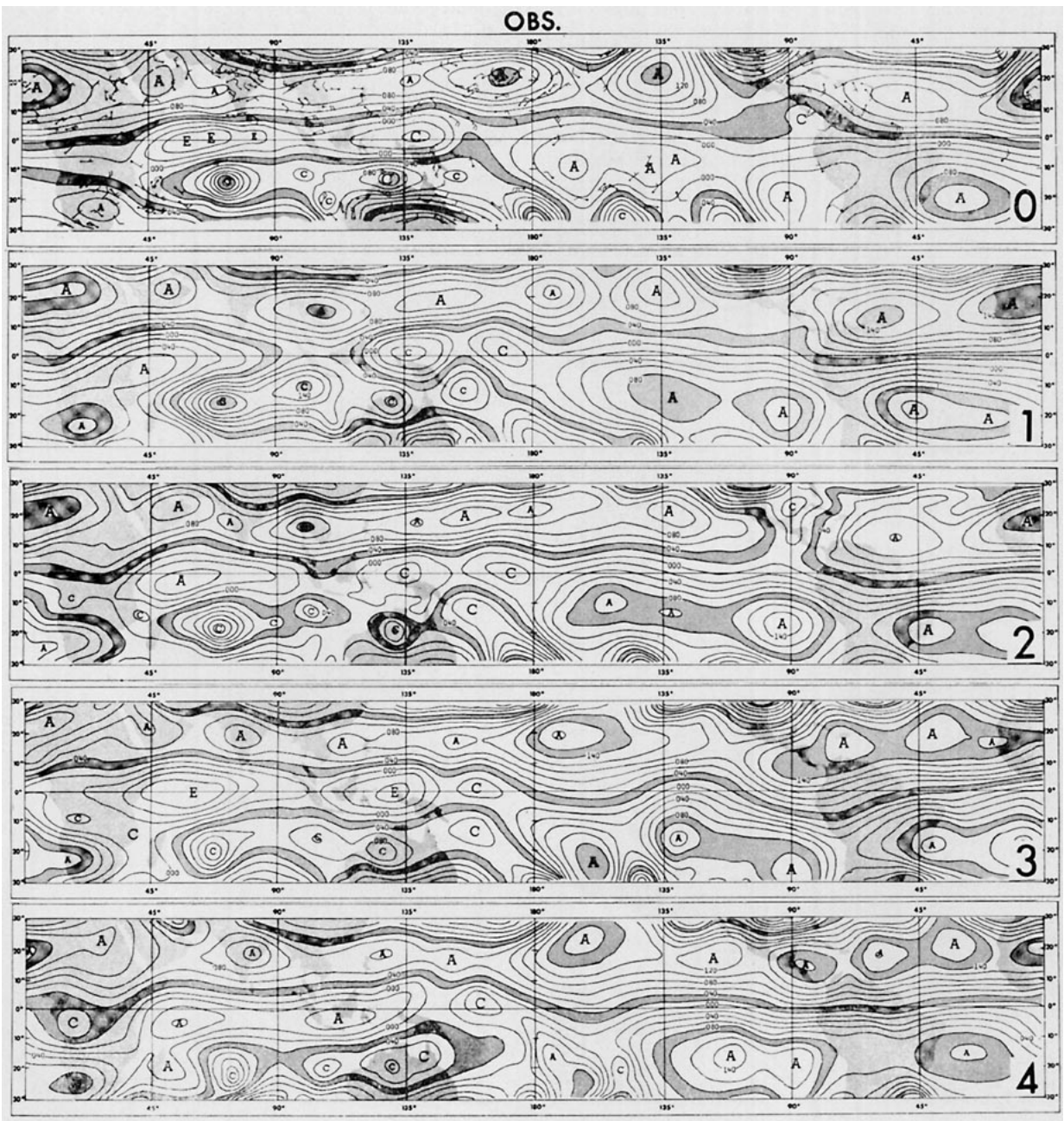

of rain at the equator is definitely due to inadequacy in the specification of the sea surface temperature distribution. In particular, the eastern and central equatorial Pacific is supposed to have a cold water pool, which does not appear in the present data. However, our results indicate that this is not the major deficiency in the model's specifications, since there is an equatorial concentration of predicted rainfall in the Indian Ocean—which has no belt of cold equatorial waters.

7. The equatorial sinking motion and heat budget

An interesting and intriguing result found in this experiment is that the mean meridional circulation reveals a tendency for downward current at the tropopause level on the equator (Fig. 8), though a dynamical significance has not yet been attached to this fact. The postulate of downward current at the equator has been proposed by two groups. In the first group are Tucker (1964), Reed (1964), and Wallace (1967), who search for the explanation of the "26-month cycle." The other group includes Fletcher (1945) and Charney (1966), who tried to show a consistent picture of the Hadley circulation with the ITC zone located away from the equator. The downward current which we are now concerned with in our experiment may be relevant to none of them. The downward current is presented almost constantly in the lower stratosphere as well as in the upper troposphere. In particular, right at the equator, the vertical flow seems to penetrate downward quite sharply with time.

Why does this motion exist and how are the heat balance and moisture balance maintained? It is known that there is a temperature minimum both in the horizontal and in the vertical at the tropical tropopause. Manabe and Hunt (1968), discussing the tropical heat budget, inferred that the minimum tempera-

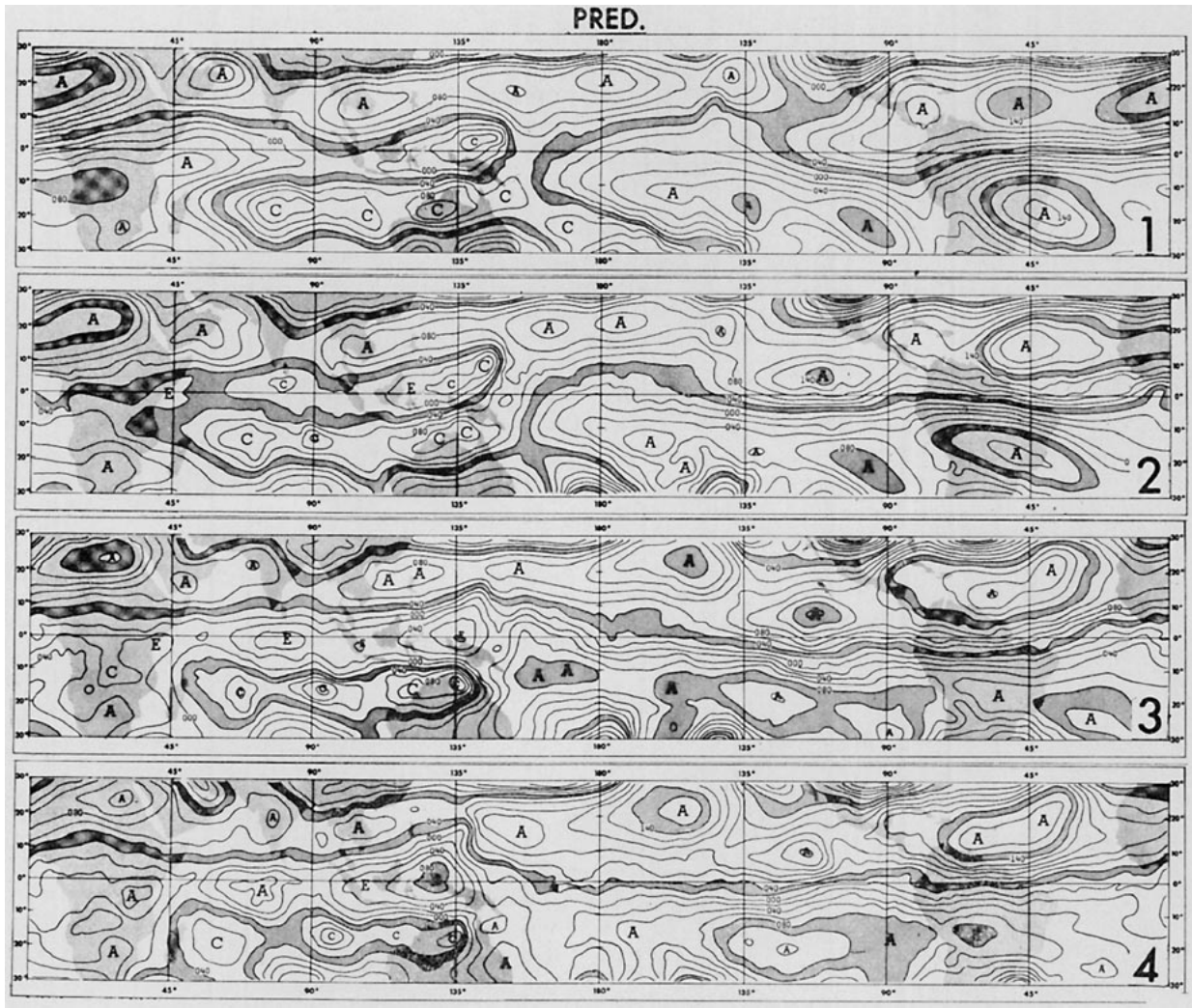

FIG. 11. Comparison of the streamfunction patterns for 4 days at the 700-mb level: forecast patterns (right) and observed (left). The station data are plotted on the 0th day map.

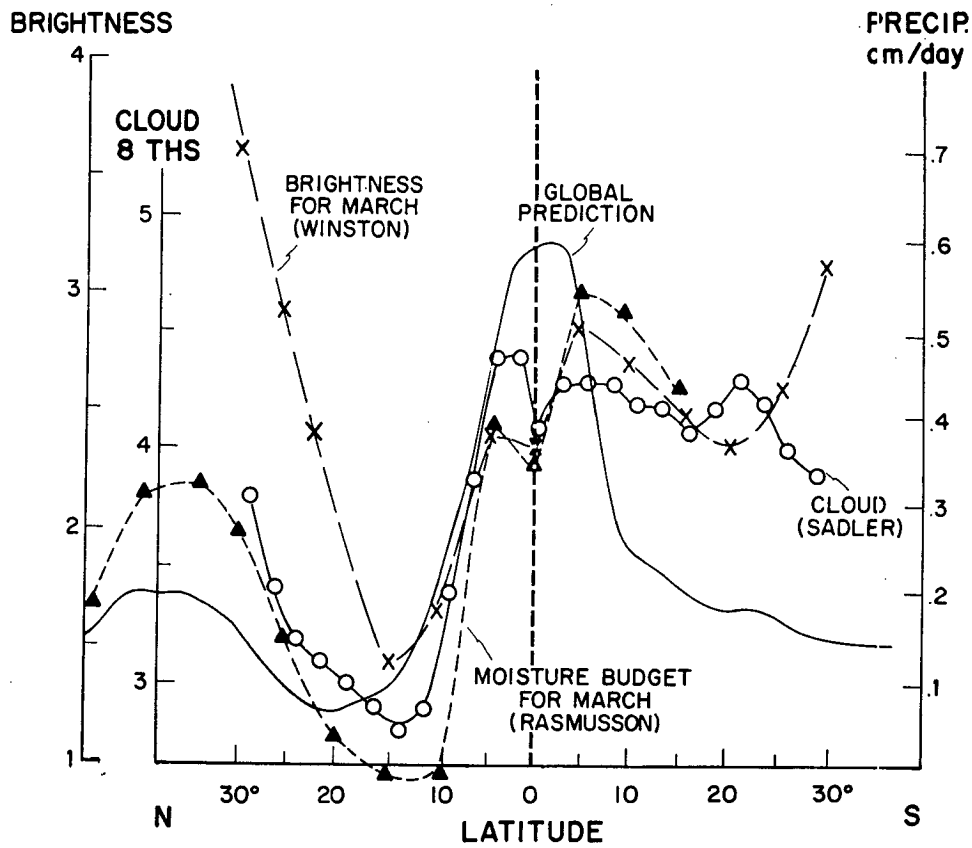

FIG. 12. Latitudinal distribution of the predicted precipitation in cm day^{-1} (solid curve, marked Global Prediction); cloudiness in octas (open circles connected with solid lines, marked Sadler); brightness (crosses connected with dashed lines, marked Winston); and the convergence of moisture flux in cm day^{-1} (triangles connected with dashed lines, marked Rasmusson).

ture at the tropopause is achieved mainly by the mean meridional circulation rather than the eddy circulation. In their case, the zonal mean vertical velocity is directed upward in the tropics and accordingly it contributes to the cooling of the tropical atmosphere. So far as the monthly mean temperature is concerned, the upward branch of the Hadley circulation appears at the 80-mb level to explain the annual variation of the latitudinal position of the equatorial temperature minimum (Reed and Vlcek, 1969).

In the present study, the temperature and the humidity distribution are not peculiar but completely normal, and yet there is this mysterious downward current at the equator. How can this seemingly contradictory situation be explained?

In order to discuss this point, let us consider the thermal equation, i.e.,

$$0=\frac{\partial(p_sT)}{\partial t}+\frac{\partial(p_sTu)}{\partial x}+\frac{\partial(p_sTv)}{\partial y}+\frac{\partial(p_sT\dot{\sigma})}{\partial \sigma}-\frac{R}{c_p}\frac{T\omega}{\sigma}-p_s\dot{q}_{\rm rad}-{}_HF_T-p_s\dot{q}_{\rm con}-{}_VF_T, \quad (7.1)$$

where T is the temperature, p_s the surface pressure, x and y are the coordinates for the longitudinal and the meridional directions, respectively, u and v are the wind components for x and y, $\dot{\sigma}=d\sigma/dt$, $p=p_s\sigma$, $\omega\equiv dp/dt$, R is the gas constant of air, c_p the specific heat at constant pressure, $\dot{q}_{\rm rad}$ the heating due to radiation, $\dot{q}_{\rm con}$ the heating from condensation, ${}_HF_T$ the contribution from the horizontal diffusion, and ${}_VF_T$ the contribution due to the vertical diffusion.

To make the discussion simple, the zonal average is applied to (7.1), and we have

$$0=\frac{\partial}{\partial t}\overline{(p_sT)}+\frac{\partial}{\partial y}\overline{(p_sTv)}+\frac{\partial}{\partial \sigma}\overline{(p_sT\dot{\sigma})}-\frac{R}{c_p}\overline{\frac{T\omega}{\sigma}}-\overline{p_s\dot{q}_{\rm rad}}-\overline{p_s\dot{q}_{\rm con}}-\overline{{}_HF_T}-\overline{{}_VF_T}, \quad (7.2)$$

where the bar denotes the zonal average.

Using the output of the prediction calculation, we estimated the vertical distribution of the terms in the above equation at the equator, averaged over the two-week period. Figure 14 contains the terms as

$\frac{1}{\bar{p}_s}\frac{\partial}{\partial t}(\overline{p_s T})$: Time change of temperature

$\frac{1}{\bar{p}_s}\left[-\frac{\partial}{\partial y}(\overline{p_s v T})-\frac{\partial}{\partial \sigma}(\overline{p_s \dot{\sigma} T})+\frac{R}{c_p}\overline{\frac{T\omega}{\sigma}}\right]$: Total circulation

$+\overline{p_s \dot{q}_{\mathrm{rad}}}/\bar{p}_s$: Radiation

$\overline{p_s \dot{q}_{\mathrm{con}}}/\bar{p}_s$: Convection

${}_H\bar{F}_T/\bar{p}_s$: Diffusion

where ${}_V\bar{F}_T$ is zero in the free atmosphere, and the summation of the last four terms is supposed to be the same as the first term. As seen in the diagram, convection contributes to the temperature increase, whereas the total circulation contributes to the temperature decrease.

In order to go one step further, the variables are divided into two; for example, $T=\bar{T}+T'$, where the prime denotes the deviation from the zonal mean. Inserting this expression for all variables into the second, the third, and the fourth terms in (7.2), we have

$$\frac{\partial}{\partial y}(\overline{p_s v T})=\frac{\partial}{\partial y}(\overline{p_s}\bar{v}\bar{T})+\frac{\partial}{\partial y}(\overline{p_s}\,\overline{v'T'})+\frac{\partial}{\partial y}(\bar{v}\overline{p_s'T'})+\frac{\partial}{\partial y}(\bar{T}\overline{p_s'v'})+\frac{\partial}{\partial y}(\overline{p_s'v'T'}), \quad (7.3)$$

$$\frac{\partial}{\partial \sigma}(\overline{p_s \dot{\sigma} T})=\frac{\partial}{\partial \sigma}(\overline{p_s}\,\bar{\dot{\sigma}}\bar{T})+\frac{\partial}{\partial \sigma}(\overline{p_s}\,\overline{\dot{\sigma}'T'})+\frac{\partial}{\partial \sigma}(\bar{\dot{\sigma}}\,\overline{p_s'T'})+\frac{\partial}{\partial \sigma}(\bar{T}\overline{p_s'\dot{\sigma}'})+\frac{\partial}{\partial \sigma}(\overline{p_s'\dot{\sigma}'T'}),$$

$$\overline{\frac{R}{c_p}\frac{T\omega}{\sigma}}=\frac{R}{c_p}\frac{\bar{T}\bar{\omega}}{\sigma}+\overline{\frac{R}{c_p}\frac{T'\omega'}{\sigma}}. \quad (7.4)$$

Among them, we first select

$H(\bar{v}\bar{T})\equiv-\frac{\partial}{\partial y}(\overline{p_s}\bar{v}\bar{T})/\overline{p_s}$: divergence of meridional transport by zonally-averaged motions

$V(\bar{\omega}\bar{T})\equiv-\frac{\partial}{\partial \sigma}(\overline{p_s}\,\bar{\dot{\sigma}}\bar{T})/\overline{p_s}$: divergence of vertical transport by zonally-averaged motions

$\frac{R}{c_p}\frac{\bar{T}\bar{\omega}}{p}$: adiabatic change due to zonally-averaged motions.

These are the contributions of the mean meridional circulation to the temperature change.

Fig. 15 shows the vertical distribution of these terms at the equator, averaged for the two-week period. In the diagram, the total addition of the above terms is shown, i.e.,

$$H(\bar{V}\bar{T})+V(\bar{\omega}\bar{T})+\frac{R}{c_p}\frac{\bar{T}\bar{\omega}}{p}. \quad (7.5)$$

The individual terms are very large, i.e., of order of magnitude 10C, but the summation is smaller by one order of magnitude; the horizontal transport and the vertical transport almost cancel each other. At the tropopause, the term representing divergence of vertical transport contributes to the temperature increase as was expected from the downward motion we are concerned with. On the other hand, the divergence of horizontal transport contributes to the temperature decrease, i.e., the transport of heat away from the equator. It should be pointed out that the contributions by eddy motion are very small. In summary, it is clear that $H(\bar{v}\bar{T})$ tends to decrease the temperature and $V(\bar{\omega}\bar{T})$ tends to increase it. Manabe and Hunt's conclusions that the contribution of the meridional circulation is far larger than that of eddy motion is true in our case, but the negative tendency of temperature is achieved by the horizontal divergence of heat transfer. It is interesting to note that Maruyama (1968), using observed data, calculated the divergence of heat flux out of the equatorial zone and obtained a significant contribution from the mixed Rossby-gravity waves to the heat budget at the tropopause level.

Thus we have a possible explanation of how the heat budget is maintained at the equator despite the sinking motion particularly at the tropopause level. However, the reason why the downward current is produced is not made clear. Furthermore, the reality of this descending motion is still questionable. One possibility is that it is the result of the "convective adjustment." Whatever the reason is, and whether or not it is real, however, the overall picture of the heat budget at the equator which was displayed above is perhaps correct.

8. Conclusions

Some capability in the prediction of day-to-day tropical troposphere flow fields is evident. The best

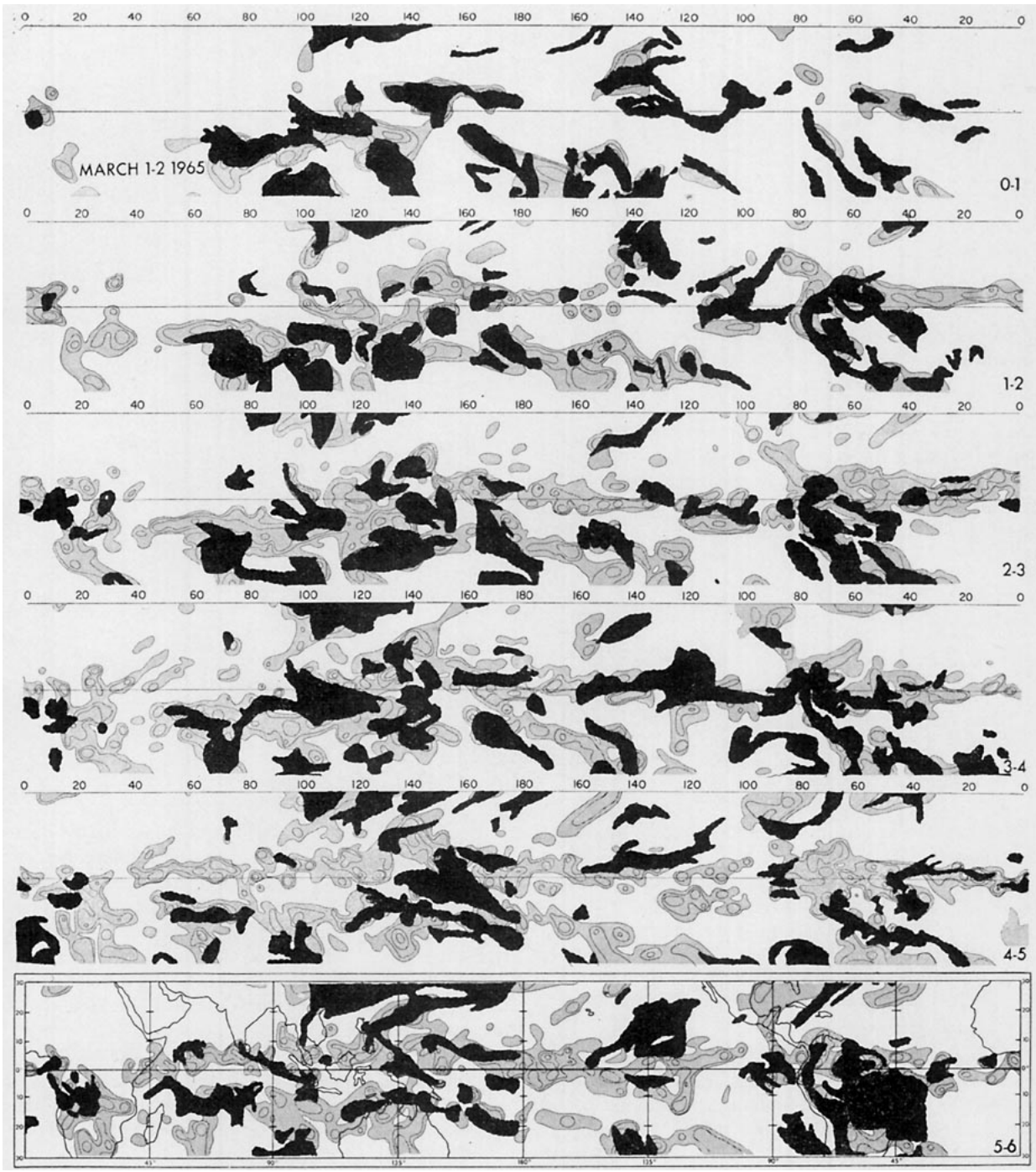

FIG. 13. Comparison of predicted rain (lightly shaded areas) and the observed cloudiness (darker areas) on the Mercator map between 30N and 30S.

simulated level appears to be the upper troposphere with less skill for higher and lower levels. In the forecasts for 700 mb, the summer monsoon westerlies of the South Indian Ocean are maintained as a recognizable current up through 3 days; however, the eastern end of the monsoon system, north and east of Australia, decays very rapidly and vanishes after day 2. The stratospheric prediction turned out to be a complete failure. Even at the 1st day, the predicted pattern of 50-mb flow is entirely different from that of the analysis. The forecast at the surface is not good. There are a number of well observed vortices, the horizontal scale of which is about 1000 km, that are rarely found in the forecast. Two tropical storms

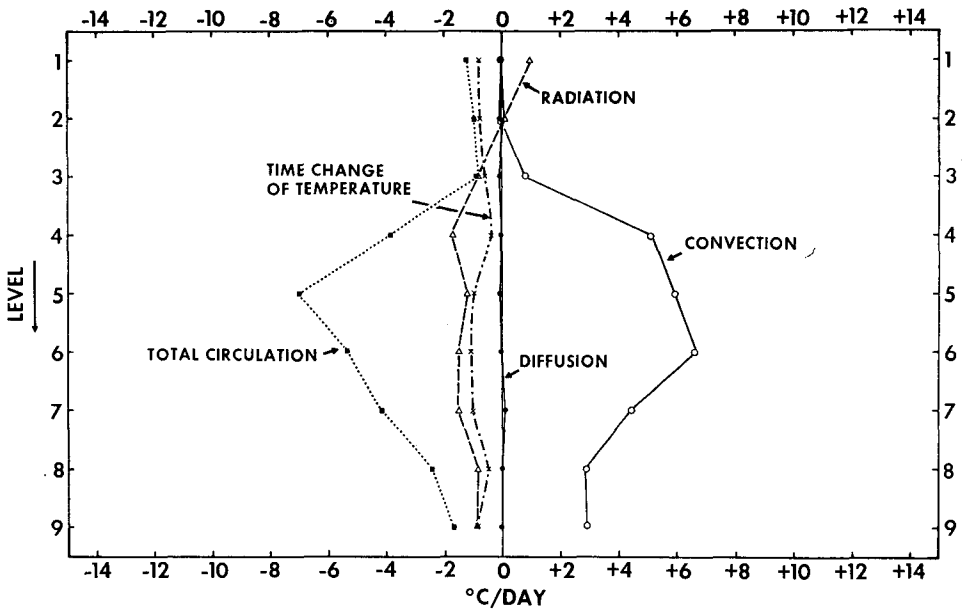

FIG. 14. Vertical distribution of the various terms in Eq. (7.2).

(hurricanes) were included in this case over the Indian Ocean. Their behavior is simulated to some extent, but the storms tend to weaken very rapidly and are very shallow. The precipitation forecast for the 1st day is surprisingly good, but it deteriorates rapidly. The predicted rain pattern appears to be erroneously spotty after about 2 days, and has undue concentration along the equator. In the zonal mean averaged for 10 days, the forecast zonal component of the wind shows a systematic bias in which the stratospheric easterlies are too strong, as are the low-level easterlies. The "Berson westerlies" above the tropopause are missing (due to the insufficient vertical resolution of the model.)

One noteworthy fact that emerged in this experiment is that a downward current exists right at the equatorial tropopause even in the zonal and temporal (10-day) mean. The temperature minimum at this level may seem to conflict with the existence of the downward current, but the heat budget can be explained without contradiction. The downward current in the zonal mean circulation tends to contribute to

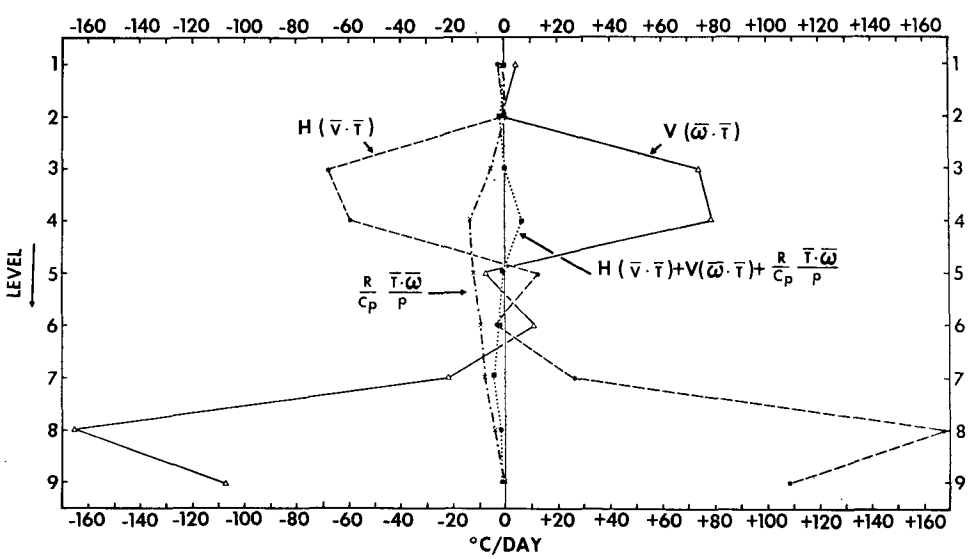

FIG. 15. Vertical distribution of some terms in Eq. (7.3), related to the mean meridional circulation.

the temperature increase, whereas the horizontal transport of heat by zonal mean motion contributes to the temperature decrease.

Thus, we conclude that the vertical grid resolution of the present prediction model is insufficient, being the main reason for the model's failure to forecast the stratosphere and to simulate the Berson westerlies. Since in the tropics the atmospheric wave motion tends to have many modes in the vertical (Lindzen and Matsuno, 1968), which was clearly evident in the Line Island Experiment (Madden and Zipser, 1970), and also since water vapor is an important element in the tropics and has large gradients in the vertical, the tropical prediction requires a great deal of vertical resolution (J. D. Mahlman, personal communication.) The considerable impact of vertical resolution on the dynamics of the tropical circulation has been studied and confirmed by comparative experiments with the 9- and 18-level models, which will be reported elsewhere. At the same time, the adequacy of the horizontal grid resolution of the model is also a problem, particularly in connection with the simulation of tropical storms. Obviously, with the 2° spacing one should not expect very much. It is our overall impression that a higher resolution is required, perhaps less than 2°, which may not be quite so stringent for forecasting at higher latitudes. Another point is that the accuracy of the initial conditions, as well as of the verification maps, should be increased and that the initialization scheme should be improved.

This is the report of our first trial for a tropical forecast. We were unable to answer all the questions posed in the introduction, which may require a number of experiments. In any event, we did learn many things from this experiment.

Acknowledgments. The authors thank Dr. J. Smagorinsky and Prof. C. S. Ramage for their continuous encouragement and help, and Messrs. R. W. Moyer, R. F. Strickler, and R. H. Clarke for assistance with this project. They also express their appreciation to Drs. Y. Hayashi, Y. Kurihara, S. Manabe, and T. C. Gordon for reviewing the paper, to Messrs. T. L. Mauk, J. T. Pollock, L. W. Reed, and I. Shulman for their help, and to Mrs. B. Williams for typing the manuscript. Finally, we thank Dr. C. W. Newton, the editor, for his special consideration of this paper.

REFERENCES

Atkinson, G. D., and J. C. Sadler, 1970: *Mean cloudiness and gradient-level-wind charts over the tropics.* AWS Technical Report 215, Vol. I and II.

Bates, J. R., 1970: Dynamics of disturbances on the Intertropical Convergence Zone. *Quart. J. Roy. Meteor. Soc.*, **96**, 677–701.

Bedient, H. A., and J. Vederman, 1964: Computer analysis and forecasting in the tropics. *Mon. Wea. Rev.*, **92**, 565–577.

Charney, J. G., 1966: Some remaining problems in numerical weather prediction. Advances in Numerical Weather Prediction, 1965–1966 Seminar Series. Hartford, Conn., The Travelers Research Center, 61–76.

Clarke, R. H., and R. F. Strickler, 1972: Southern hemisphere prediction experiment with a nine-level, primitive equation model. *Mon. Wea. Rev.*, **100**, 625–636.

Fletcher, R. D., 1945: The general circulation of the tropical and equatorial atmosphere. *J. Meteor.*, **2**, 167–174.

Gadd, A. J., and J. F. Keers, 1970: Surface exchanges of sensible and latent heat in a 10-level atmosphere. *Quart. J. Roy. Meter. Soc.*, **96**, 297–308.

Gray, W. M., 1968: Global view of the origin of tropical disturbances and storms. *Mon. Wea. Rev.*, **96**, 669–700.

Hayashi, Y., 1971: Frictional convergence due to equatorial waves in a finite-depth Ekman layer. *J. Meteor. Soc. Japan*, **49**, 450–457.

Hayden, C. M., 1970: An objective analysis of cloud cluster dimension and spacing in the tropical North Pacific. *Mon. Wea. Rev.*, **98**, 534–540.

Holloway, J. L., Jr., and S. Manabe, 1971: Simulation of climate by a global general circulation model. I. Hydrologic cycle and heat balance. *Mon. Wea. Rev.*, **99**, 335–370.

Holton, J. R., J. M. Wallace, and J. A. Young, 1971: On boundary layer dynamics and the ITCZ. *J. Atmos. Sci.*, **28**, 275–280.

Kidson, J. W., D. G. Vincent, and R. E. Newell, 1969: Observational studies of the general circulation of the Tropics; long term mean values. *Quart. J. Roy. Meteor. Soc.*, **95**, 258–287.

Krishnamurti, T. N., 1969: An experiment in numerical prediction in equatorial latitudes. *Quart. J. Roy. Meteor. Soc.*, **95**, 594–620.

——, 1971: Observational study of tropical upper tropospheric motion field during the Northern Hemisphere summer. *J. Appl. Meteor.*, **6**, 1066–1096.

——, and W. J. Moxim, 1971: On parameterization of convective and non-convective latent heat release. *J. Appl. Meteor.*, **10**, 3–13.

Kurihara, Y., 1965: Numerical integration of the primitive equations on a spherical grid. *Mon. Wea. Rev.*, **93**, 399–415.

——, and J. L. Holloway, Jr., 1967: Numerical integration of a nine-level global primitive equations model formulated by the box method. *Mon. Wea. Rev.*, **95**, 509–530.

Lindzen, R. S., and T. Matsuno, 1968: On the nature of large-scale wave disturbances in the equatorial lower stratosphere. *J. Meteor. Soc. Japan*, **46**, 215–221.

Madden, R. A., and E. J. Zipser, 1970: Multi-layered structure of the wind over the equatorial Pacific during the Line Islands Experiments. *J. Atmos. Sci.*, **27**, 336–342.

Malkus, J., 1962: Large-scale interactions. In *The Sea: Ideas and Observations*, M. N. Hill, Ed. New York, Wiley Interscience. **1**, 88–294.

Manabe, S., J. Smagorinsky, and R. F. Strickler, 1965: Simulated climatology of a general circulation model with a hydrologic cycle. *Mon. Wea. Rev.*, **93**, 769–798.

——, and B. G. Hunt, 1968: Experiments with a stratospheric general circulation model: I. Radiative and dynamic aspects. *Mon. Wea. Rev.*, **96**, 477–502.

——, J. L. Holloway, Jr., and H. M. Stone, 1970: Tropical circulation in a time-integration of a global model of the atmosphere. *J. Atmos. Sci.*, **27**, 580–613.

——, ——, and D. Hahn, 1974: The seasonal variation of the tropical circulation as simulated by a global model of the atmosphere. *J. Atmos. Sci.*, **31**, 43–83.

Maruyama, T., 1968: Upward transport of westerly momentum due to large scale disturbances in the equatorial lower stratosphere. *J. Meteor. Soc. Japan*, **45**, 404–417.

Matsuno, T., 1966: Numerical integrations of primitive equations by use of a simulated backward difference method. *J. Meteor. Soc. Japan*, **44**, 76–84.

Miller, B. I., 1969: Experiment in forecasting hurricane development with real data. Tech. Memo. ERITM-NHRL 85, National Hurricane Research Laboratory, NOAA, 28 pp.

Miyakoda, K., 1960: Numerical solution of the balance equation. Tech. Rep., Japan. Meteor. Agency, No. 3.

——, R. W. Moyer, H. Stambler, R. H. Clarke, and R. F. Strickler, 1971: A prediction experiment with a global model of the Kurihara-grid. *J. Meteor. Soc. Japan*, **49**, Special Issue, 521–536.

——, J. Smagorinsky, R. F. Strickler, and G. D. Hembree, 1969: Experimental extended predictions with a nine-level hemispheric model. *Mon. Wea. Rev.*, **97**, 1–76.

——, R. F. Strickler, C. J. Nappo, P. L. Baker, and G. D. Hembree, 1971: The effect of horizontal grid resolution in an Atmospheric Circulation model. *J. Atmos. Sci.*, **28**, 481–499.

Oort, A. H., and E. M. Rasmusson, 1970: On the annual variation of the monthly mean meridional circulation. *Mon. Wea. Rev.*, **98**, 423–442.

Ooyama, K., 1969: Numerical simulation of the life cycle of tropical cyclones. *J. Atmos. Sci.*, **26**, 3–40.

Pike, A. C., 1972: Response of a tropical atmosphere and ocean model to seasonally variable forcing. *Mon. Wea. Rev.*, **100**, 424–433.

Rasmusson, E. M., 1973: Seasonal variation of tropical humidity parameters. *General Circulation of Tropical Atmosphere*, Vol. I, R. F. Newell, J. W. Kidson, D. G. Vincent, and G. J. Boer, Eds. Cambridge MIT Press.

Reed, R. J., 1964: A tentative model of the 26-month oscillation in tropical latitudes. *Quart. J. Roy. Meteor. Soc.*, **90**, 441–466.

——, and C. L. Vlcek, 1969: The annual temperature variation in the lower tropical stratosphere. *J. Atmos. Sci.*, **26**, 163–167.

Riehl, H., 1954: *Tropical meteorology*. New York, McGraw-Hill, 392 pp.

Sadler, J. C., 1957: Wind regimes of the troposphere and lower stratosphere over the equatorial and sub-equatorial Central Pacific. *Proc. of Ninth Pac. Sci. Cong.*, Vol. 13, pp. 6–11, Bangkok, Thailand.

——, 1965: The feasibility of global tropical analysis. *Bull. Amer. Meteor. Soc.*, **46**, 118–130.

——, 1969: Average cloudiness in the Tropics from satellite observations. *International Indian Ocean Expedition Meteorological Monographs*. No. 2, Honolulu, Hawaii, East-West Center Press, 22 pp.

——, 1972: The mean winds of the upper troposphere over the central and eastern Pacific. UHMET 72-04 and ENVPREDSCHFAC Tech. Paper No. 8-72. Honolulu, Hawaii, University of Hawaii.

——, and B. E. Harris, 1970: The mean tropospheric circulation and cloudiness over Southeast Asia and neighboring areas. Hawaii Institute of Geophysics, Report HIG-70-26 and AFCRL-70-0489. Honolulu, Hawaii, University of Hawaii.

Smagorinsky, J., S. Manabe, and J. L. Holloway, Jr., 1965: Numerical results from a nine-level general circulation model of the atmosphere. *Mon. Wea. Rev.*, **93**, 727–768.

Tucker, G. B., 1964: Zonal wind over the equator. *Quart. J. Roy. Meteor. Soc.*, **90**, 405–423.

Vanderman, L. W., 1972: Forecasting with a global, three-layer, primitive-equation model. *Mon. Wea. Rev.*, **12**, 856–868.

Wallace, J. M., 1967: On the role of mean meridional circulation in the biennial wind oscillation. *Quart. J. Roy. Meteor. Soc.*, **93**, 176–185.

Wetherald, R. T., and S. Manabe, 1972: Response of the joint ocean-atmosphere model to the seasonal variation of the solar radiation. *Mon. Wea. Rev.*, **100**, 42–59.

Winston, J. S., 1971: The annual course of zonal mean albedo as derived from ESSA 3 and 5 digitized picture data. *Mon. Wea. Rev.*, **99**, 818–827.

Yamasaki, M., 1971: A further study of wave disturbances in the conditionally unstable model tropics. *J. Meteor. Soc. Japan*, **49**, 391–415.